Dual phase renewable fuel combustion in an atmospheric gas turbine burner

Ogbonnaya Agwu[a,*], Jon Runyon[a], Burak Goktepe[a], Cheng Tung Chong[b], Jo-Han Ng[c], Anthony Giles[a], Agustin Valera-Medina[a]

[a]*School of Engineering, Cardiff University, Wales, UK*

[b]*China-UK Low Carbon College, Shanghai Jiao Tong University, Lingang, Shanghai, China*

[c]*Faculty of Engineering and Physical Sciences, University of Southampton Malaysia, Malaysia*

*Corresponding author. Email: AgwuOE@cardiff.ac.uk

Abstract

Expanding the fuel flexibility of continuous combustion systems to include multiphase fuel combustion offers additional support to combat the problem of energy security and, potentially, environmental pollution. In this study, apart from establishing stability limits and measuring post-combustion emissions, flames generated from simultaneous combustion of biodiesel and syngas were examined using C_2* and CH* chemiluminescence imaging to capture changes in the reaction zone. The proportion of syngas in the fuel mix was varied from 0-30% content (by energy contribution) while maintaining a total power output of 15 kW and global equivalence ratio of 0.7 in all cases except for determining the flammability range. The results indicate a reduction of stability limits as gas proportion in fuel blend increases. Also, chemiluminescence imaging of the two targeted species suggest a general reduction in reaction rate as well as reaction zone area and length with increase in gas ratio in the dual phase tests. Furthermore, emissions performance in the context of NO_X and CO was investigated as liquid-to-gas ratios were altered. Conclusively, the study demonstrates the feasibility, limitations and potential benefits of multiphase renewable fuel burn in a swirl-stabilised atmospheric burner.

Keywords: dual fuel, gas turbine, multiphase, combustion

1. Introduction

Energy consumption is both the stimulus for and consequence of economic development. As a result, energy security – the uninterrupted availability of energy – is to the economy of nations what food security is to its health. However, economic expansion has an inverse relationship with the quantity of non-renewable energy reserves. At the same time, never has the need to green the energy industry been more urgent. As such, alternative sources of energy, particularly those of the renewable kind, have been explored to avoid over-reliance or complete dependence on a single source. Accordingly, fuel flexibility is an increasingly attractive attribute of secondary

energy generators such as reciprocating engines and continuous combustion devices. Fuel flexibility in such systems not only entails the ability of burning a wide variety of fuels individually but also the capability for simultaneous combustion of multiple fuels in different phases.

Consequently, there has been, in recent times, research into multiphase fuel combustion in continuous combustion systems. One of the earliest published studies, conducted by Sidey and Mastorakos [1], examined ethanol-methane-air flames in a swirl-stabilised atmospheric burner. Using Mie scattering, OH* chemiluminescence and OH-PLIF imaging, they determined the effect on flame structure and stability as the fraction of gas in the fuel combination was altered. They reached the conclusion that flame stability is negatively perturbed as methane fraction in combusted fuel increases. A similar conclusion was reached by the same authors [2] when they studied *n*-heptane-methane-air flames using the same burner configuration and visualisation techniques of their previous study. Also, Evans *et al.* [3] showed the extent of flame temperature and reaction zone structure variation on *n*-heptane-methane/hydrogen flames using the non-linear excitation regime two-line atomic fluorescence and OH-PLIF techniques.

More practical gas turbine fuels have also been studied. For example, Chong *et al.* [4] investigated palm biodiesel co-combustion with natural gas in a swirl stabilised burner using CH* and OH* chemiluminescence. Following on from that study, Chiong *et al.* [5] sought to know the influence of swirler vane angle on the biodiesel/natural gas co-combustion in terms of emissions and reported lower NO emissions at larger swirl vane angles. Also, Agwu and Valera-Medina [6] studied the simultaneous combustion of fossil diesel and syngas in a swirl-stabilised atmospheric burner. In addition to stable flame operating range and flame stability, post combustion emissions were also measured in those studies. Moreover, Agwu *et al.* [7] carried out a similar study: waste oil derived biodiesel flames burning in air premixed with varying amounts of methane. The last two mentioned studies generally showed that with increasing gas amounts in the combustion air stream, flame stability is improved while the range of stable flame operation is reduced when the dual fuel flames are compared with neat liquid fuel combustion. Further, with recent interest in ammonia because of its carbon-free nature and potential renewability, Okafor *et al.* [8] investigated the combustion of liquid ammonia in a single stage swirl combustor and reported enhanced combustion of the fuel and reduced flame heights with the addition of methane.

The above reviewed research regarding simultaneous combustion of liquid and gas fuels in continuous combustion devices does not represent the entirety of multi-fuel combustion in such systems. In fact, as shown in Table 1, majority of studies in simultaneous fuel combustion in continuous reacting flow systems involves blends of fuels in the same phase (liquid/liquid and gas/gas). These single-phase dual fuel combustion cases abound ranging from diesel and glycerol blends to wood liquefied in alcohols. From Table 1, it is clear that continuous flow combustors

like the gas turbine enjoy extensive multi-fuel flexibility albeit skewed towards single phase fuel blends.

Table 1. Multi-fuel combustion tests in gas turbine type combustors in the last decade

Fuels tested	*Engine type*	*Injection strategy*	*Power output*	*Equivalence ratio*	*Research interest*	*Researcher(s)*	*Date*
CH_4, CO_2 and O_2	Model swirl burner	Partially premixed	10 – 30 kW	0.5 - 1	Flame stability and operability with oxyfuel combustion	Kutne *et al.* [9]	2011
Blends of jatropha biodiesel and diesel	IS/60 rovers gas turbine	-	44 kW	Variable	Feasibility of jatropha biodiesel as GT fuel	Rehman *et al.* [10]	2011
Wood liquefied in poly hydroxyl alcohols	Swirl burner	Air-blast atomiser		Variable	Feasibility of liquefied wood as GT fuel	Seljak *et al.* [11]	2012
N_2, CO_2, steam and syngas (H_2 and CO)	Model GE7EA industrial gas turbine; 1 atm, 500^0C inlet conditions	-	60 kW	Variable	Combustion performance of syngas and effect of dilution of other gases	Lee *et al.* [12]	2012
Biodiesel and vegetable oil blends	Garett GTP 30-67 micro gas turbine	Pressure atomiser	0 – 25 kW	Variable	Exhaust emissions performance in comparison with diesel	Chiaramonti *et al.* [13]	2013
Rapeseed and sunflower oil and Jet A1 kerosene blends	Capstone micro gas turbine model C30	Air-blast atomiser	15, 25 kW	Variable	Exhaust emissions investigation	Chiariello *et al.* [14]	2014
Butanol and Jet A blends	University of Oklahoma propulsion Lab gas turbine	-	30 kW	0.18 – 0.33	Performance and emission characterisation	Mendez *et al.* [15]	2014
Biodiesel and pyrolysis oil blends	Generic swirl burner	Pressure atomiser	3 – 60 kW	0.5 – 1.4	Emissions performance with alternative fuels	Kurji *et al.* [16]	2016
CO2/CH4/biodiesel and CO2/CH4/diesel	Model swirl burner	Pressure atomiser	20 kW	1.4 – 2.2	Multiphase combustion trial in gas turbines	Kurji *et al.* [17]	2017
Jet A-1 and hydrotreated renewable jet fuel blends	Gas turbine swirl burner (Cardiff GTRC)	Pressure atomiser	41 kW	0.8 – 1.1	Operability and fuel performance of gas turbine with the fuel blend	Buffi *et al.* [18]	2017
Ammonia and methane	Gas turbine swirl burner (Cardiff GTRC)	Premixed	30 kW	0.8 – 1.45	Flame stability and emissions study	Valera-Medina *et al.* [19]	2017
Butyl butyrate and ethanol blends	Aero engine-based GT burner with intake pressure (0 – 7 MPa) and inlet temperature up to 600 K	-	-	variable	Gaseous and PM emissions study	Chen *et al.* [20]	2017

Table 1. *continued*.

Fuels tested	*Engine type*	*Injection strategy*	*Power output*	*Equivalence ratio*	*Research interest*	*Researcher(s)*	*Date*
Ethanol and methane	Model atmospheric bluff-body burner	Pressure atomiser; Partially premixed	Variable	variable	Flame structure and stability investigation	Sidey and Mastorakos [1]	2017
Jatropha biodiesel and diesel blends	Model swirl GT with inlet temperature of 600 K	Air-blast atomiser	40 kW	0.5 – 2.0	Operability and emissions performance of gas turbine with the alternative fuels	Bhele *et al.* [21]	2018
Fast pyrolysis bio-oil and ethanol blends	Capstone micro gas turbine model C30 LF	Pressure swirl atomiser	5 – 20 kW	Variable	Investigation of viscous fuel use as blend component in micro gas turbine	Buffi *et al.* [22]	2018
n-heptane and methane	Model atmospheric bluff-body burner	Pressure atomiser; Partially premixed	Variable	0.31 – 0.66	Flame structure and stability characteristics of dual fuel flames	Sidey and Mastorakos [2]	2018
Hydrogen-ammonia blends	Gas turbine swirl burner (Cardiff GTRC)	Premixed	39.3 kW	0.9 – 1.4	Investigating the complexity of burning ammonia in blends with hydrogen	Valera-Medina *et al.* [23]	2019
Diesel and glycerol	Micro gas turbine	Pressure atomiser	3 – 6 kW	Variable	Combustibility and characteristics of glycerol combustion emissions	Seljak and Katrašnik [24]	2019
Natural gas and n-heptane	Model atmospheric bluff-body burner	Pressure atomiser; Partially premixed	Up to 6 kW	Variable	Temperature distribution and reaction zone characteristics	Evans *et al.* [3]	2019
Diesel and syngas	Model swirl burner	Pressure atomiser	6 – 20 kW	Variable	Multiphase combustion trial in gas turbines	Agwu and Valera-Medina [6]	2020
Methane and ammonia blends	50 kW model swirl burner	Premixed and non-premixed	50 kW	Variable	Emissions production and control in methane-ammonia flames	Okafor *et al.* [25]	2020
Biodiesel and methane	Model swirl burner	Pressure atomiser and non-premixed	6 – 20 kW	Variable	Multiphase fuel burn in continuous flow systems	Agwu *et al.* [7]	2020
Glycerol and methanol	Model swirl burner	Pressure atomiser and non-premixed	6 kW	0.29 – 0.51	Multiphase fuel burn in continuous flow systems	Agwu *et al.* [26]	2020
Liquid ammonia and methane	Model gas turbine swirl combustor	Pressure atomiser and non-premixed	-	0.8 – 1.2	Liquid ammonia co-combustion with methane	Okafor *et al.* [8]	2021

As far as the authors know, previous research has not explored multiphase renewable fuel combustion in continuous flow systems. Consequently, the current paper investigates the co-combustion of two renewable fuels – biodiesel and syngas – in a swirl-stabilised atmospheric burner. The gaseous fuel was premixed with the combustion air in the burner plenum prior to the introduction of the liquid fuel. The amount of gaseous fuel utilised at any one time was varied to deliver between 10% and 30% of the total heat output of 15 kW. This study compares the different multiphase fuel combustion cases with the corresponding liquid fuel burn in three areas: stable flame operating range using the flame extinction method; reaction zone properties and flame stability using data from CH* and C_2* species chemiluminescence and post combustion emissions of CO and NO_X.

2. Methodology and Considerations

2.1 Burner and fuel supply

The dual fuel atmospheric swirl burner and associated fuel delivery system utilised for this study is described in Agwu *et al.* [7]. A 3D rendition of the burner as well as a 2D section of it are shown in Fig. 1. Air was metered by means of a variable area rotameter with an accuracy ±5% at full scale deflection for the air flow. The syngas flow rates were controlled by a Bronkhorst EL-Flow Prestige MFC with an accuracy of ±0.5% of the indicated reading. The gas/air mixture passes through a 5-vane axial swirler prior to entering the combustion chamber. The gaseous fuel and air were supplied to the system at ambient temperature while the biodiesel was injected using a Delavan 0.4 GPH 60^{o}W pressure-swirl nozzle. It has the smallest orifice of all Delavan nozzles and was selected because of the relatively low liquid flow rates encountered in the study.

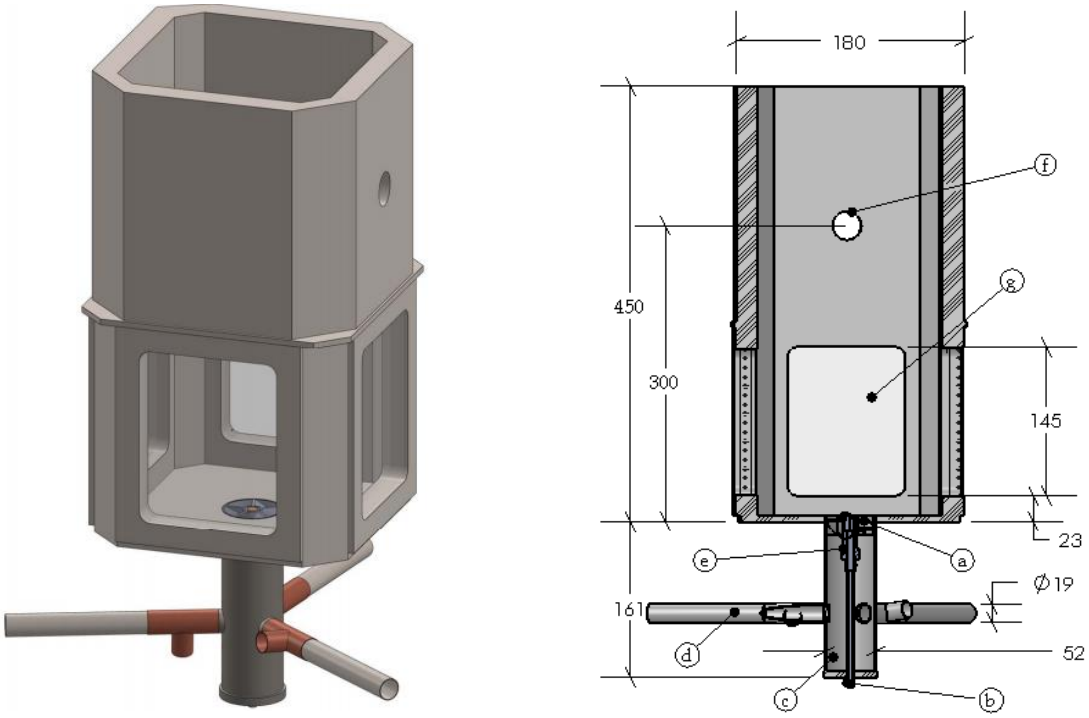

Fig. 1. (left) 3D CAD of burner set-up (right) 2D section view showing (a) axial swirler (b) liquid fuel line (c) inlet plenum (d) combustion air/syngas inlet (e) pressure atomiser (f) emissions probe slot (g) quartz window. All dimensions in millimetres.

2.2 Fuel properties and test operating conditions

The physical and chemical characteristics of the fuels used in the study are provided in Table 2 with biodiesel data from Chong and Hochgreb [27] and Kumar *et al.* [28]. The biodiesel used in the study was sourced from Olleco, UK, who describe it as methyl esters from lipid sources produced per EN14214 standard. The model syngas, subsequently referred to simply as 'syngas', was made up of 10% hydrogen, 10% carbon monoxide and 80% methane by volume. Based on mole fraction composition, the density, lower heating value and stoichiometric fuel/air ratio (FAR) for the syngas shown in Table 2 were determined.

Table 2. Properties of tested fuels.

Property	Biodiesel	Syngas
Lower heating value, LHV (MJ/kg)	36.8	43.8
Density (kg/m^3)	880	0.671
Surface tension, σ (*kg/s^2*)	0.032*	-
Kinematic viscosity, ν (*mm^2/s*)	6.75*	-
FAR (stoichiometric)	0.080	0.068

The stoichiometric FAR (on a mass basis) for biodiesel was calculated based on the ideal combustion equation: $C_{19}H_{36}O_2 + 27(O_2 + 3.76N_2) \rightarrow 19CO_2 + 18H_2O + 101.52N_2$. On the other hand, the FAR of syngas was calculated based on the ideal combustion equations of each

of its constituents: $CH_4 + 2O_2 \rightarrow CO_2 + 2H_2O$; $H_2 + 0.5O_2 \rightarrow H_2O$ and $2CO + O_2 \rightarrow 2CO_2$ taking into account the molar concentration of each constituent.

The specific syngas composition was selected because it results in gas with both a stoichiometric fuel-air ratio and lower heating value (LHV) similar to that of biodiesel. This is important because syngas with a very dissimilar FAR to biodiesel and/or a very different LHV will cause a correspondingly different overall gas (air and syngas) flow rate across the various fuel blends tested. The changing gas flow rates will, in turn, perturb both the isothermal and reacting flow dynamics to varying degrees across the test cases thereby making comparison of different performance indices difficult across the test cases. An illustration of the potential perturbances of the non-reacting flow dynamics is shown in Fig. 2 which is a CFD simulation of non-reacting flow through the burner at varying air flow rates.

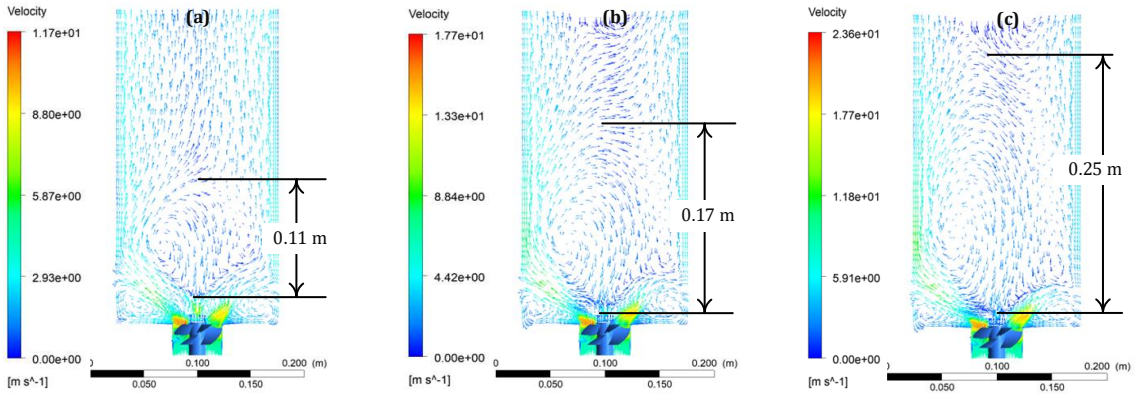

Fig. 2. Non-reacting gas flow velocity contours for 90/10 LGR at (a) experimental flowrate (b) 1.5 times experimental flowrate (c) twice experimental flowrate.

Apart from the relatively large variation in the range of flow velocities across the different simulated cases (see colour bars), there is a noticeable alteration in the size of the central recirculation zone (CRZ) formed, particularly the length, as a result of the swirling in the flow. The CRZ is well known to encourage flame stability as it enables recirculation of the hot combustion products so that the incoming fuel/air mixture can be anchored and sustained [29]. Therefore, variations in its size in non-reacting conditions will affect the reacting flow characteristics which are of interest in this study. To minimise this, the syngas composition was selected so that comparable overall gas flow rates are achieved as indicate in Table 3. A simulation of these flow rates across the burner is shown in Fig. 3 and indicates a non-reacting flow zone that is relatively constant as liquid/gas ratio (LGR) is altered. It is important that the cold flow dynamics across the test cases be maintained if differences in flame structure, stability and other performance parameters are to be attributed to the fuel composition.

The numerical calculation whose results are shown in Fig. 2 and Fig.3 were obtained from simulating swirling non-reacting flows using the finite-volume based commercial CFD package, ANSYS Fluent 2019 R1. The geometry forming the computation domain, Fig. 4.1 (a), was designed using Solidworks 2019. Ansys Fluent's task-based workflow for watertight geometries was utilised for meshing using the following steps: CAD import, surface mesh, geometry description, flow-volume extraction and then volume meshing. To confirm grid independence, three different meshes with varying number of cells were tested. In each of the three mesh sizes, grid size was refined in the area containing the swirler to better capture fluid dynamics there and the grid quality was over 0.25 in all cases. For the flow simulation, a RANS model (realizable k-ε) was employed to describe the flow field solving conservation equations for mass and momentum. The governing equations were solved implicitly using the finite volume method in which a second order scheme was used for spatial discretization. A key component of the combustor utilised for the experimental studies is the 5-vane axial swirler that is fitted with its top surface flush with the nozzle exit plane and dump plane of the burner. A three-dimensional model of the swirler was designed and incorporated into the 3-D CFD simulation of the air flow through the system. The total mass of fluid present in the domain was tracked and used to monitor convergence.

Table 3. Fuel composition and operating conditions at a total power output of 15 kW and $\varphi_{global} = 0.7$. *determined experimentally.

LGR	Biodiesel/syngas flow rates			ΔP (*MPa*)
	Biodiesel	Syngas	Air	
100/0	0.41	0	7.28	0.85
90/10	0.37	0.03	7.27	0.75
80/20	0.33	0.07	7.26	0.60
70/30	0.29	0.10	7.25	0.38

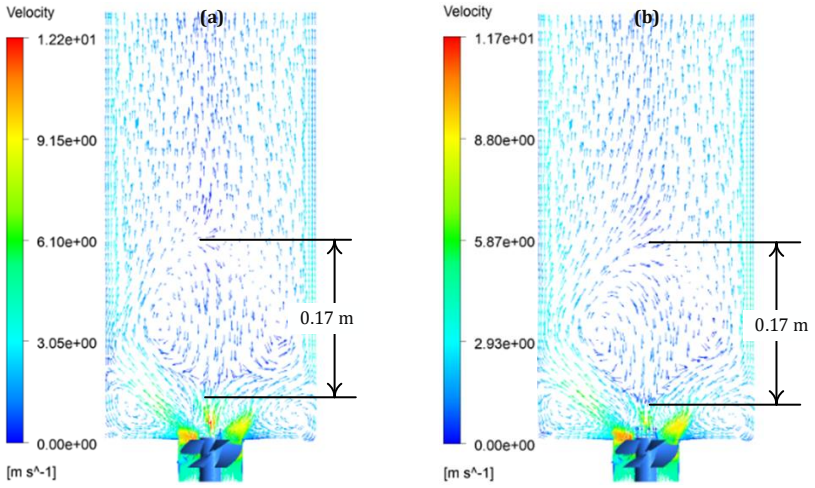

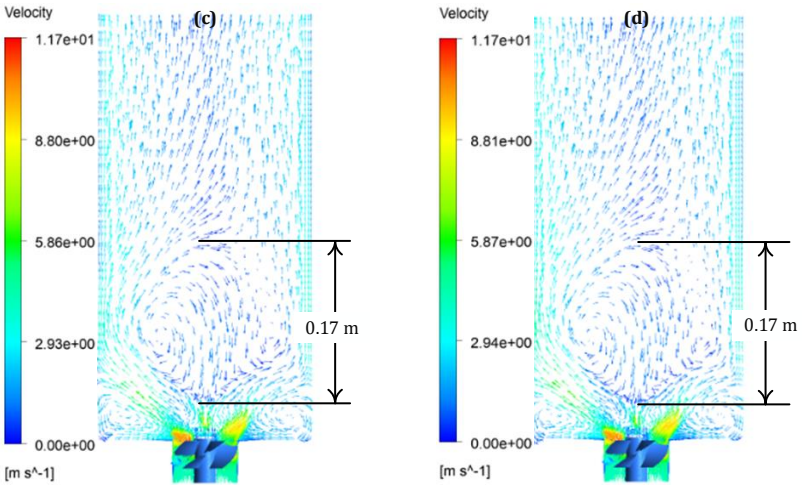

Fig. 3. Velocity contours with the size of the CRZ highlighted for (a) 100/0 (b) 90/10 (c) 80/20 and (d) 70/30 overall gas flow rates.

The liquid/gas ratio (LGR) of combusted fuel was based on energy share ratio, similar to the method used in Dimitriou *et al.* [30], and altered from 100/0 to 70/30. A liquid/gas ratio of 80/20, for instance, would mean that the liquid fuel supplies 80% of the total heat output (THO) and the remainder is supplied by the gas. Except for flame extinction measurements, the combination of the two sets of fuels were set to deliver a THO of 15 kW based on LHV of the fuels and calculated using Eq. (1) where $\dot{m}$ signifies the mass flow rate of fuel and the subscripts *l* and *g* represent liquid and gas, respectively. The relevant premixed swirling air flow rate was calculated according to Eq. (2) with φ_{global} signifying global equivalence ratio, kept constant at 0.7 for the tests.

$$THO = (LHV_l \times \dot{m}_l) + \left(LHV_g \times \dot{m}_g\right) \quad (1)$$

$$\dot{m}_{air} = \frac{\dot{m}_g \times AFR_{Stoic,g} + \dot{m}_l \times AFR_{Stoic,l}}{\varphi_{global}} \quad (2)$$

2.3 Emissions measurement methods

Flame optical emissions, namely C_2* and CH* radicals, were obtained by chemiluminescence imaging. These species were targeted as they are indicative of heat release rate in hydrocarbon flames according to Kathrotia *et al.* [31] and García-Armingol *et al.* [32]. The imaging set-up was as follows: A LaVision highspeed IRO intensifier coupled to a 60 mm focal length AF Micro-Nikkor (f/2.8) lens and mounted onto a LaVision Imager Intense CCD camera. The camera was focused at the centreline of the burner capturing a plane that is ±50 mm in the radial direction and ±140

mm in the axial direction with the setup resulting in a resolution of 0.12 mm/pixel. Optical access is possible only after the first 23 mm from the burner dump plane, so in the resulting images the 0 mm mark refers to the start of optical access. A bandpass filter centred at 515 nm (Full width at half maximum, FWHM = 10 nm) was installed on the intensifier to transmit one of the C_2* chemiluminescence swan bands. The selected band is spectrally resolved with an easily observable peak near the selected filter centre for liquid fuelled combustors as shown in [32] and [33]. Similarly, to measure CH* chemiluminescence, a bandpass filter centred at 430 nm (FWHM = 10 nm) was used. For further information about the chemiluminescence set-up and data acquisition and processing, refer to [6] and [7].

Flue gas emissions measurements were made using a Testo 350 XL emissions analyser the probe of which was positioned at the mid-point of the burner 300 mm downstream of the nozzle orifice plane. The control unit of the analyser was set to sample flue gas for two minutes for each test condition at a rate of 3 seconds per measurement. Of the resulting 40 readings, the last 20 were averaged and reported. With a reaction time of 40 s and 30 s for CO and NO_X measurements respectively, the readings settled well before the last 20 readings. All readings were taken at an oxygen reference of 15% while equipment calibration indicates an uncertainty estimation of ±0.2% for oxygen and ±5% measurement uncertainty for the emissions reported.

3 Results and discussion

3.1 Stable operation range

The stable operating bounds, following the method described by Lefebvre and Ballal [34], were identified noting the lean and rich extinction limits of the combusted fuel, and the results are displayed in Fig. 4 for the biodiesel/syngas flames.

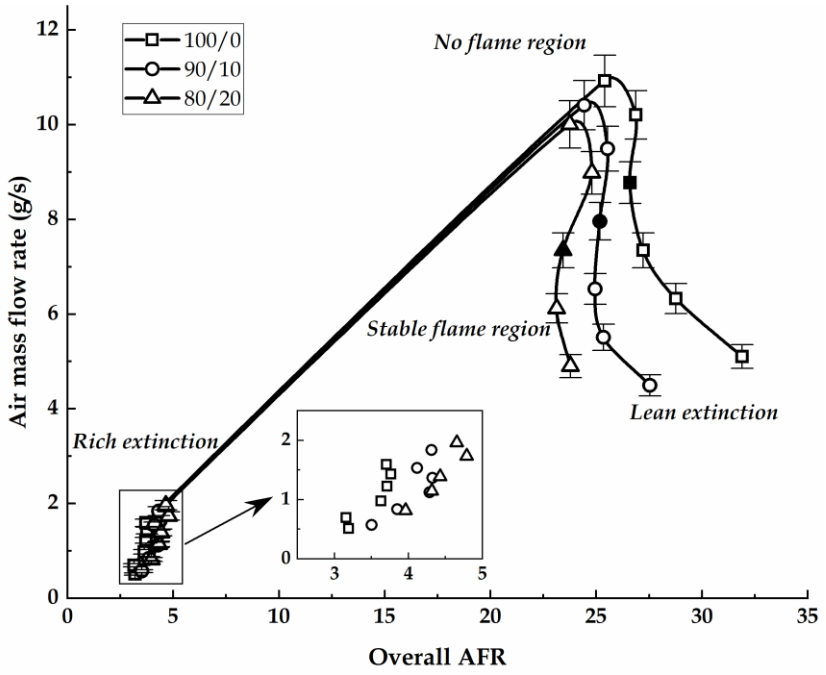

Fig. 4. Operability range of burner for three different biodiesel/syngas blends.

The 'lean extinction' section indicates the maximum air mass flow rate and overall air-to-fuel ratio (AFR) attainable for a specific power output delivered by the neat liquid fuel or a combination of liquid and gaseous fuels. There is also a corresponding point for rich extinction at the same power output. This process was repeated for several power outputs within the range 8 – 18 kW allowing for a delineation of the region within which stable burning can be achieved as indicated in Fig. 4. This region of stable burning, the area beneath the curve of Fig. 4, gets progressively smaller as the gaseous fuel partly replaces the liquid fuel in the combustion process. A comparison of equivalence ratio range between the rich and lean limits at a heat output of 12 kW (the solid points in Fig. 4) reveals that there is a 27.6% reduction in flammable equivalence ratio range between the 100/0 and 80/20 case for the biodiesel/syngas flame.

The change in stability limits as gas content of fuel blend rises is attributable to at least two factors. The first has to do with the deteriorating liquid fuel spray quality as LGR decreases as shown in Fig. 5. The fuel droplet Sauter mean diameter (SMD) values in Fig. 5 were obtained from Radcliffe's SMD correlation (Eq. 3), proven by Alsulami *et al.* [35] to yield the best predictions for SMD of spray droplets for the pressure-swirl nozzle utilised in the present study.

$$SMD = 7.3{\sigma_l}^{0.6}{\nu_l}^{0.2}{\dot{m}_l}^{0.25}\Delta P^{-0.4} \quad (3)$$

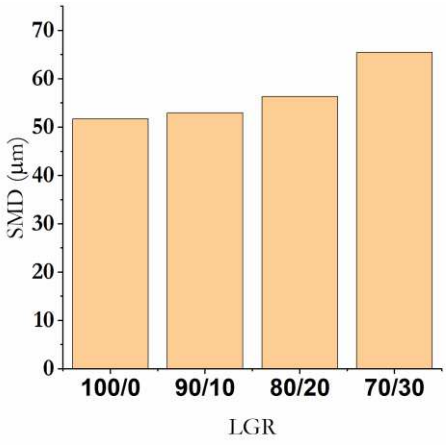

Fig. 5. Variation in biodiesel SMD values based on Radcliffe's correlation as LGR changes.

The pressure drops (ΔP) across the nozzle, provided in Table 3, was measured downstream of the MFC just before nozzle. The other variables of Eq. (4), $\dot{m}_l$, σ_l and ν_l are the liquid mass flow rate, surface tension and kinematic viscosity respectively. These values can be found in Tables 2 and 3. The SMD trend shown in Fig. 5 results in declining combustion efficiency, certainly in terms of the liquid fuel which contributes the majority of the heat output in each extinction test, even as gas content of fuel blend increases. The relatively larger droplet sizes as LGR decreases do not support combustion as much as the finer sprays at higher LGR thus contributing to the reduction in stability limits observed in Fig. 4. At an LGR below 80/20, flames were difficult to establish and could not be sustained over most of the range of THO used in plotting the flammability limits most likely because of the noted deterioration of liquid fuel atomisation quality. As a result, the 70/30 combination was omitted from this analysis.

The other contributing factor to the decreasing range of stable flame operation in both multiphase combustion cases as LGR decreases is the alteration in reacting flow dynamics revealed by the CH* and C_2* species chemiluminescence images. The changes in the RZ properties as well as the spatial distribution of the excited radical combustion species, based on the chemiluminescence images (section 3.2), suggests that the reacting flow pattern is perturbed as gas is introduced into the combustion process. At a low gas fraction (90/10), it would seem that the gas is able to diffuse well into the biodiesel spray while at higher gas fractions, its combustion is localized. Regardless, the effect of these changes in reacting flow dynamics is the reduction in flammable range following the method used here for establishing the stable range of operation. The method increases or reduces air flow rate until extinction occurs thereby determining a range of air/fuel combinations that permits combustion and is different from flame stability at a fixed operating point which is determined later.

The general reduction in stability limits noted here highlights an important operational consideration for multiphase fuel combustion employed in swirl-stabilised combustion systems: combustion cannot be maintained over as wide a range of AFRs as it would for neat liquid fuel burn.

3.2. Optical Emissions and Flame Characteristics

The C_2* and CH* chemiluminescence images normalised to the highest intensity in each category of the different combinations of biodiesel/syngas are presented in Fig. 6 at THO = 15 kW and φ_{global} = 0.7. The chemiluminescence profiles indicate, among the dual phase cases, a shortening of the RZ length as LGR is decreased. The images also show that as the gas content of combusted fuel increases, the C_2* and CH* emissions intensity diminish accompanied by a lateral extension of the RZ area close to the nozzle orifice plane.

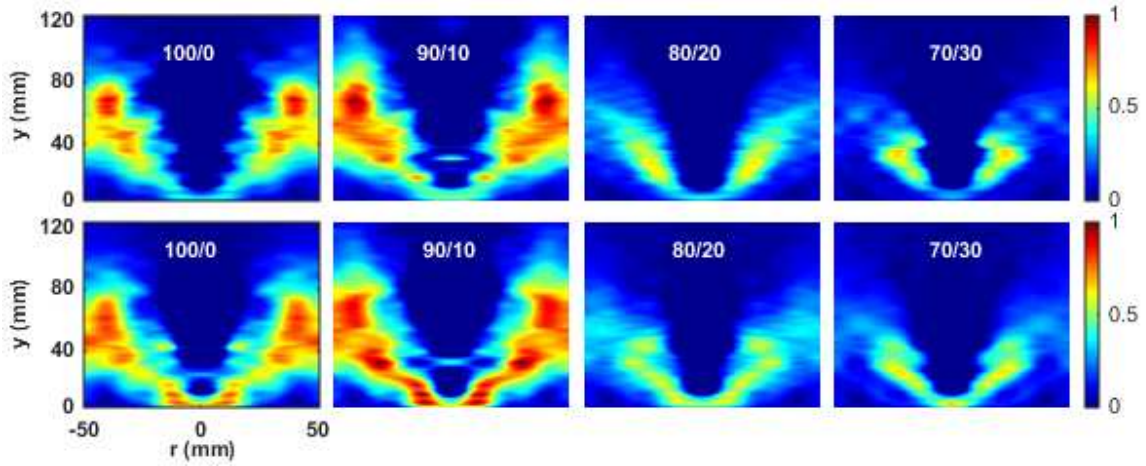

Fig. 6. *Top*: Abel-transformed C_2* chemiluminescence of biodiesel/syngas flame normalised by the maximum C_2* chemiluminescence intensity across the different compositions. Bottom: Abel-transformed CH* chemiluminescence of biodiesel/syngas flame normalised by the maximum CH* chemiluminescence intensity across the different compositions.

To evaluate and characterize quantitatively the reaction zone property changes as LGR changes, the chemiluminescence images of Fig. 6 were binarized. Conversion of the chemiluminescence images to binary images was done using the Otsu thresholding method and the results are shown in Fig. 7. The Otsu thresholding method is suitable here because it selects a threshold value that minimises the intraclass variance of the black and white pixels. The threshold value was determined separately in the 100/0 image for each of the two chemiluminescence species and subsequently held constant across the test cases in each category. The binary images offer an insight into the reaction zone (RZ) area and length.

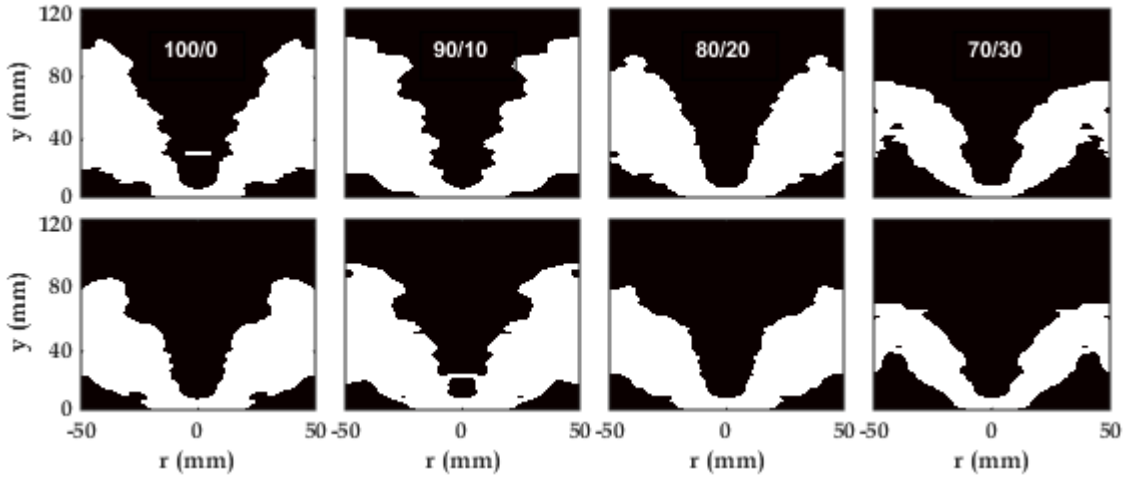

Fig. 7. Binary images of C2* (top row) and CH* (bottom row) chemiluminescence in biodiesel/syngas flames at different liquid/gas ratios. Flow is from bottom to top.

The summation of the unity pixels in the binary images are used as a representation of the RZ area whereas the RZ length is estimated as equal to the distance between the uppermost and lowermost unity pixel of each binary image along the vertical axis. A quantitative description of the variation in RZ properties is shown in Fig. 8. The general trend in the multiphase cases is that as gas fraction increases, both reaction zone area and length reduce. Compared to neat biodiesel combustion however, a 90/10 blend of biodiesel/syngas demonstrates greater reaction zone length and area. The reason for this is probably because at very low percentages in the intake air, the syngas mixture is too fuel-lean to form a distinct combustion regime as is possible at higher gas fractions. This was noticeable in the physical observation of the flames and in the luminosity images (shown in Fig. 9). Instead of forming its own combustion zone, the ultra-lean gas at 90/10 LGR diffuses into the biodiesel spray and thereby promoting a larger combustion zone. As a consequence, the RZ length and area of the biodiesel/syngas flames at an LGR of 90/10 appears greater than of neat biodiesel (LGR = 100/0) combustion as seen in Fig. 8. As gas fraction increases and the intake air is richer in syngas, a separate combustion regime close to the nozzle exit plane forms. This combustion regime is predominantly a syngas flame and the heat produced encourages early onset of liquid fuel combustion and as a result, imparts an overall shorter reaction zone length and smaller reaction zone area.

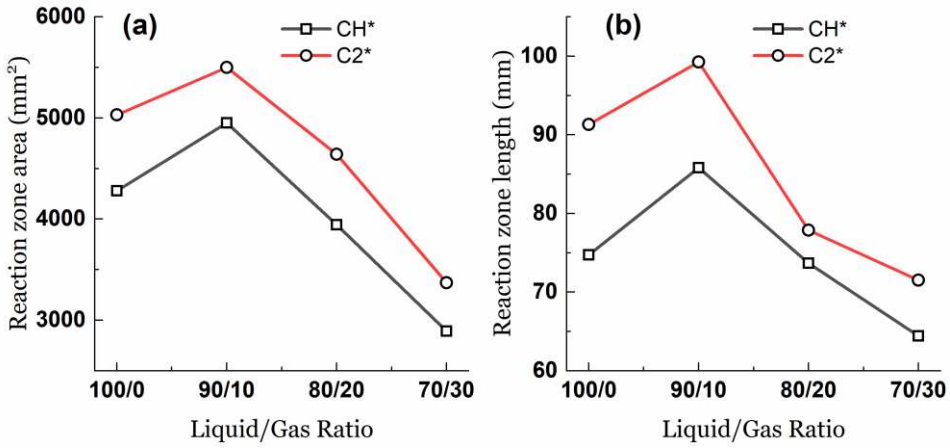

Fig. 8. Reaction zone characteristics for different blends of biodiesel/syngas

Both the reacting flow dynamics captured by the chemiluminescence images and the trend of RZ properties shown in Fig. 8 were observed in earlier studies. For example, Evans *et al.* [3] noted similar variation in the appearance of swirling n-heptane-NG/H_2 flames claiming that fuel was being drawn out from the inner reaction zone to the outer branch of the flame. Also, flame property variation similar to those in the present study were observed in the earlier studies of diesel/syngas flames studied in [6] and biodiesel/methane flames of [7].

In addition to the reacting flow dynamics variation theory proffered by [3], the flame structure variation can also be attributed to the adopted injection strategy for both fuels. For one, the gaseous fuel is premixed with the oxidiser and although locally lean, it enhances combustion within what may be considered the primary zone of the combustor by encouraging early reaction in the flow. This is evident in the luminosity images of Fig. 9 in which the flame is all but separated from the orifice plane in the 100/0 case but progressively gets more attached and spread out close to the orifice plane. Seen clearly in the 70/30 case is a bluish flame right next to the orifice plane pointing to lean combustion of the syngas early in the combustion process.

100/0 90/10 80/20 70/30

Fig. 9. Biodiesel/syngas flame luminosity images

Over and above that, the pressure atomiser used for injecting the liquid fuels had earlier been shown to deliver poorer spray quality as LGR decreases. Towards the lower end of the LGRs tested, the deterioration of spray quality results in larger droplets which require relatively longer evaporation timescales that is not attainable for all droplets given the relatively early reaction initiated by the gaseous fuel. In addition, the air further downstream of the gas combustion zone is vitiated in oxygen having participated in the earlier, predominantly syngas, combustion. As a consequence, not only does overall reactivity (radical species integral intensity) decrease but also RZ area and length diminishes.

3.3. Flame stability at a single operating point

Further processing of the chemiluminescence images was carried out to evaluate the stability of the individual flames at a global equivalence ratio of 0.7 and an overall power output of 15 kW. The method used here tracks the C_2* and CH* integral intensity over the duration of their capture before evaluating the temporal variation of each chemiluminescence intensity. The chemiluminescence intensity at any instance is representative of the heat release rate (HRR) at that point so that the temporal variation of the radical species concentration indicates the HRR fluctuation which in turn gives an indication of the stability state of the flame [36].

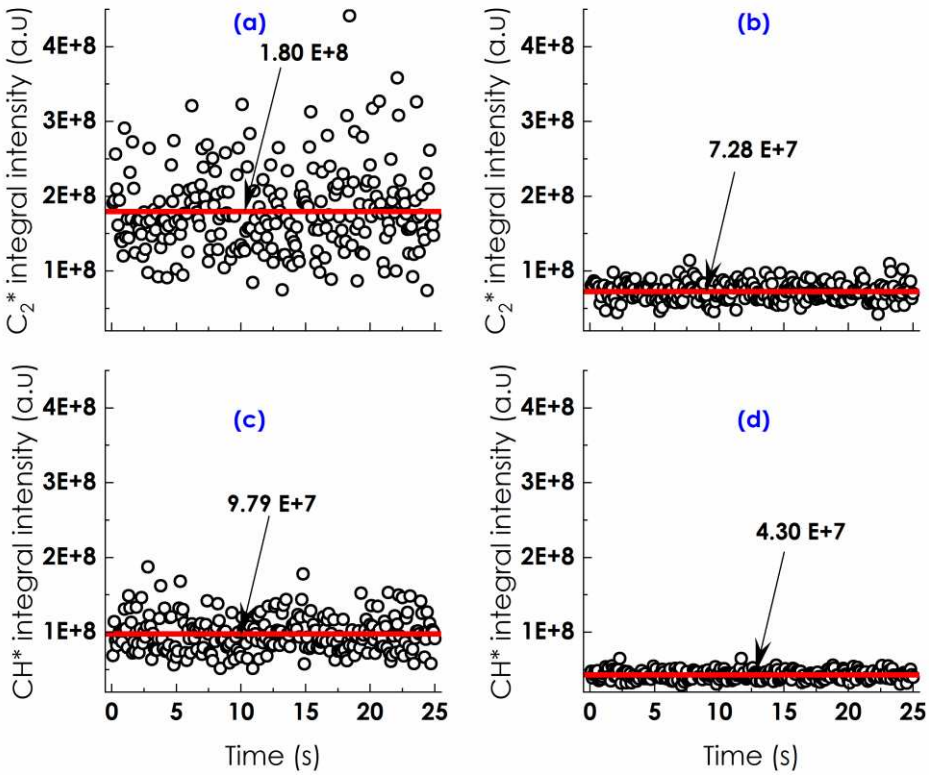

Fig. 10. Temporal variation of C_2* species integral intensity for (a) 100/0 (b) 70/30 and CH* species integral intensity for (c) 100/0 (d) 70/30 biodiesel/syngas flames.

Fig. 10 shows the C_2* and CH* integral intensity fluctuation for the 100/0 and 70/30 biodiesel/syngas flames while. Clearly, there is a greater fluctuation in integral intensity values in the 100/0 case compared to the 70/30 case indicating increased flame stability in the latter case. Also, moving from the time domain of Fig. 10 to a frequency domain using fast Fourier transform (FFT), the same conclusion can be drawn (see Fig. 11).

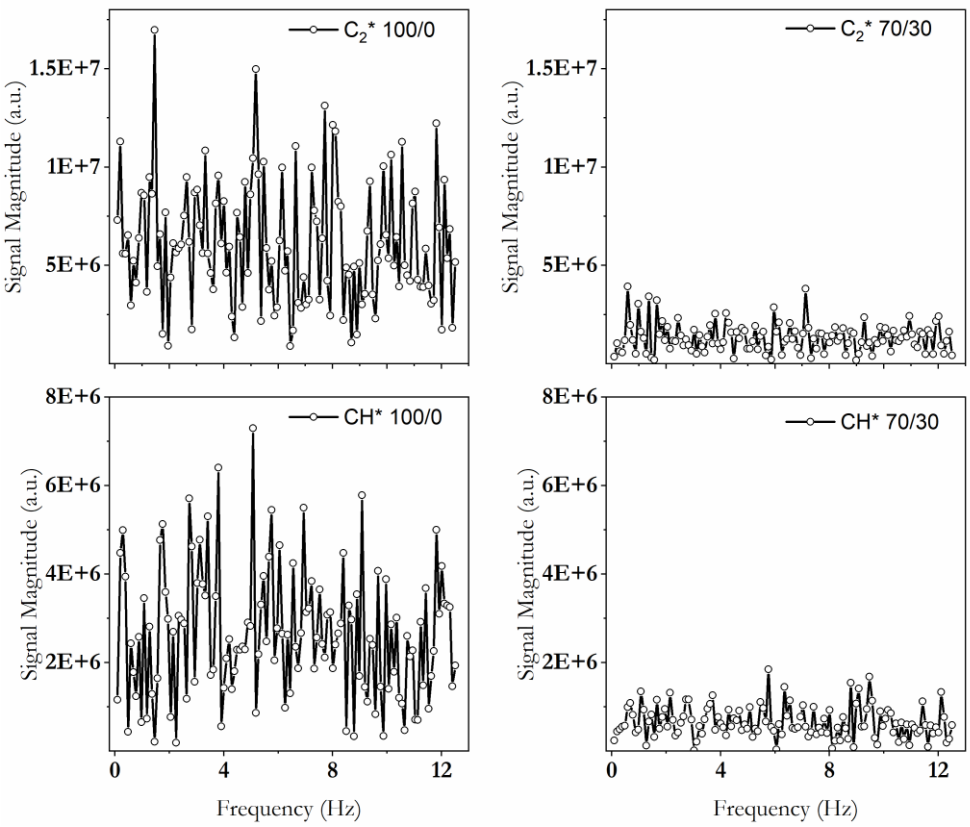

Fig. 11. Frequency variation of C_2* species integral intensity for (a) 100/0 (b) 70/30 and CH* species integral intensity for (c) 100/0 (d) 70/30 biodiesel/syngas flames using FFT.

Like the time-domain signals, the frequency-domain signals have been plotted to the same scale in each of the chemiluminescence species categories to enable easier comparison. In this case, an attenuation of frequency amplitudes is observed in the 70/30 case compared with the 100/0 case indicating that there are fewer alternating periods of high and low frequency in the latter which is consistent with the time-domain representation of the signal intensities.

Going back to Fig. 10, the solid red horizontal line in the figure is the average integral intensity when the entire dataset of 250 images is considered. Because of the differences in this average intensity value for the four test conditions, comparison of the data by the method standard deviation will lead to biased results. Therefore, the coefficient of variation (CoV), the standard deviation normalized by the mean value, was used to assess the temporal variability of the radical species hence the flame stability in each test case. This information is presented in Fig. 12. The slight increase in the CoV at 90/10 LGR for the biodiesel/syngas blend is likely due to the nature of the syngas because it was also observed in the diesel/syngas blend reported in [6] but not in the biodiesel/methane case of [7]. Barring the peculiar 90/10 biodiesel/syngas blend, flame stability will be influenced by the fact that with increasing gas ratio, a lean premixed gas fuel combustion regime develops near the nozzle orifice plane, providing heat to the base of the flame in addition to that from recirculating hot products. This serves to improve flame anchoring

over and above that possible with the non-premixed combustion regime in the neat liquid fuel cases. The formation of a lean gaseous fuel combustion regime at the nozzle exit plane as observed in this study was reported by a previous study [7].

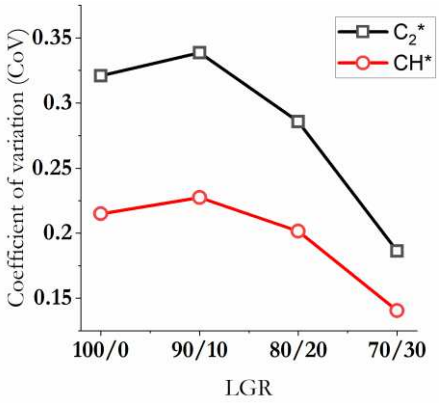

Fig. 12. Measure of temporal fluctuation of heat release rate for biodiesel/syngas flames at different LGRs.

3.4. Post combustion emissions

The NO_X and CO emissions from the four blends of biodiesel/syngas are presented in Fig. 13 with the error bars being the 5% uncertainty in the readings as stated by the calibration document from the equipment. NO_X emissions are known to depend a great deal on flame temperatures for which the rate of heat release from the fuel is key [37]. This is mirrored in the NO_X emissions data of Fig. 13 where the 90/10 blend has higher NO_X emissions than the 100/0 case and as gas rates rise above 10%, NO_X emissions fall accordingly. Relatively lower CO emissions result from biodiesel and biodiesel/syngas combustion but there is a consistency in that the CO trend is opposite that of NOx between all points. As NOx increases between 100/0 and 90/10, CO emissions fall and even though very little CO is produced in the multiphase cases, the trend is yet opposite to that of NO_X. This is because, the conditions that are favourable for NO_X production – higher temperatures/higher heat release rates – mitigate the generation of CO hence the opposite gradients.

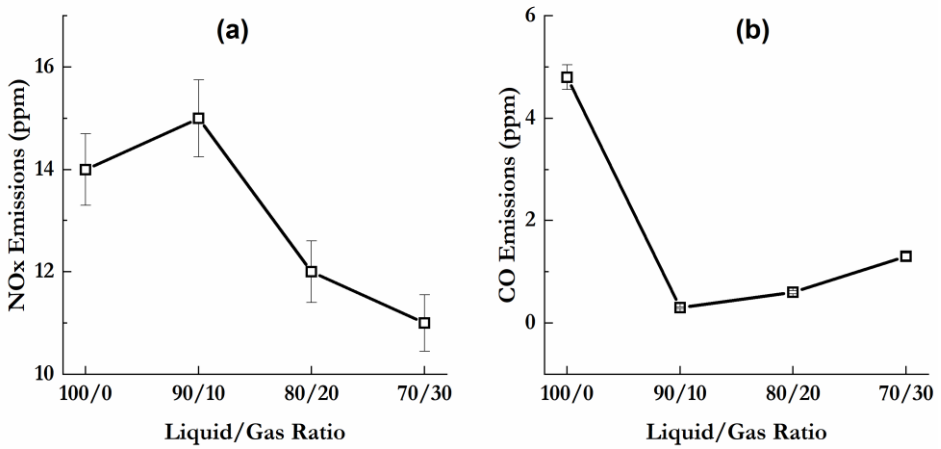

Fig. 13. Post combustion emissions from biodiesel/syngas flames at different liquid-gas ratios.

4. Conclusions

The feasibility and performance of multiphase renewable fuel combustion in a swirl-stabilised atmospheric burner was investigated using biodiesel/syngas blends. The strategy employed for simultaneous combustion of both liquid and gas type fuels was to introduce the gas premixed with the air stream and delivered through a swirler into the combustion domain where the liquid fuel is sprayed via a pressure atomiser. While maintaining total heat output, the energy share contributed by the liquid fuel was reduced to 70% in steps of 10% by substituting with gaseous fuel. The main findings from the study are:

1. Dual phase fuel combustion narrows the stability limits achievable in combustion when compared with neat liquid fuel burn. For instance, at a total heat output of 12 kW, switching from neat biodiesel to an 80/20 blend of biodiesel/syngas resulted in a 27.6% reduction in stable operating range. This effect is attributed to the variation in reacting flow dynamics coupled with liquid fuel spray quality deterioration which in turn leads to a reduction of evaporation rate as LGR decreases.
2. In the dual phase tests, the rate of heat release as well as combustion reaction zone length and area, evaluated by C_2* and CH* chemiluminescence, generally diminish as a biodiesel was increasingly replaced by a syngas in the combustion process.
3. Comparing the multiphase cases in the tests, the temporal variation of heat release rate fluctuation showed a declining trend as the gas content of the fuel blend increased. This signifies an improvement in flame stability as more of the liquid fuel is replaced with a gaseous fuel. An important reason for flame stability improvement is because there is a shift from non-premixed with the neat biodiesel to partially premixed combustion in the multiphase cases. As the syngas content increases, it tends to increasingly combust near

in the primary zone of combustion thereby adding to the heat in this zone which makes for greater flame stability in the process.

4. Increasing the fraction of heat output supplied by a gaseous fuel in the dual phase flames considered results in declining NOx emissions but increasing CO emissions. NO_X emissions reduced from 15 ppm to 11 ppm comparing the 90/10 instance to the 70/30 case while CO emissions, over the same LGR range, there rose from 0.3 ppm to 1.3 ppm.

Acknowledgements

Malcolm Seaborne, Paul Malpas and the rest of Cardiff University's Mechanical Engineering Laboratory and Workshop Technicians are gratefully acknowledged. Many thanks to Franck Lacan of the Additive Manufacturing unit of Cardiff University for printing the swirler used. Also, Ogbonnaya Agwu would like to express appreciation to the Petroleum Technology Development Fund (PTDF) Nigeria for funding his PhD at Cardiff University.

References

[1] Sidey J and Mastorakos E. *Visualisation of turbulent swirling dual-fuel flames.* Proceedings of the Combustion Institute, 2017. **36**(2): p. 1721-1727.

[2] Sidey JAM and Mastorakos E. *Stabilisation of swirling dual-fuel flames.* Experimental Thermal and Fluid Science, 2018. **95**: p. 65-72.

[3] Evans MJ, Sidey JAM, Ye J, Medwell PR, Dally BB, and Mastorakos E. *Temperature and reaction zone imaging in turbulent swirling dual-fuel flames.* Proceedings of the Combustion Institute, 2019. **37**(2): p. 2159-2166.

[4] Chong CT, Chiong M-C, Ng J-H, Tran M-V, Valera-Medina A, Józsa V, and Tian B. *Dual-Fuel Operation of Biodiesel and Natural Gas in a Model Gas Turbine Combustor.* Energy & Fuels, 2020. **34**(3): p. 3788-3796.

[5] Chiong M-C, Valera-Medina A, Chong WWF, Chong CT, Mong GR, and Mohd Jaafar MN. *Effects of swirler vane angle on palm biodiesel/natural gas combustion in swirl-stabilised gas turbine combustor.* Fuel, 2020. **277**: p. 118213.

[6] Agwu O and Valera-Medina A. *Diesel/syngas co-combustion in a swirl-stabilised gas turbine combustor.* International Journal of Thermofluids, 2020. **3-4**.

[7] Agwu O, Runyon J, Goktepe B, Chong CT, Ng J-H, Giles A, and Valera-Medina A. *Visualisation and performance evaluation of biodiesel/methane co-combustion in a swirl-stabilised gas turbine combustor.* Fuel, 2020. **277**.

[8] Okafor EC, Yamashita H, Hayakawa A, Somarathne KDKA, Kudo T, Tsujimura T, Uchida M, Ito S, and Kobayashi H. *Flame stability and emissions characteristics of liquid ammonia spray co-fired with methane in a single stage swirl combustor.* Fuel, 2021. **287**: p. 119433.

[9] Kutne P, Kapadia BK, Meier W, and Aigner M. *Experimental analysis of the combustion behaviour of oxyfuel flames in a gas turbine model combustor.* Proceedings of the Combustion Institute, 2011. **33**(2): p. 3383-3390.

[10] Rehman A, Phalke DR, and Pandey R. *Alternative fuel for gas turbine: Esterified jatropha oil–diesel blend.* Renewable Energy, 2011. **36**(10): p. 2635-2640.

[11] Seljak T, Rodman Oprešnik S, Kunaver M, and Katrašnik T. *Wood, liquefied in polyhydroxy alcohols as a fuel for gas turbines.* Applied Energy, 2012. **99**: p. 40-49.

[12] Lee MC, Seo SB, Yoon J, Kim M, and Yoon Y. *Experimental study on the effect of N2, CO2, and steam dilution on the combustion performance of H2 and CO synthetic gas in an industrial gas turbine.* Fuel, 2012. **102**: p. 431-438.

[13] Chiaramonti D, Rizzo AM, Spadi A, Prussi M, Riccio G, and Martelli F. *Exhaust emissions from liquid fuel micro gas turbine fed with diesel oil, biodiesel and vegetable oil.* Applied Energy, 2013. **101**: p. 349-356.

[14] Chiariello F, Allouis C, Reale F, and Massoli P. *Gaseous and particulate emissions of a micro gas turbine fuelled by straight vegetable oil–kerosene blends.* Experimental Thermal and Fluid Science, 2014. **56**: p. 16-22.

[15] Mendez CJ, Parthasarathy RN, and Gollahalli SR. *Performance and emission characteristics of butanol/Jet A blends in a gas turbine engine.* Applied Energy, 2014. **118**: p. 135-140.

[16] Kurji H, Valera-Medina A, Runyon J, Giles A, Pugh D, Marsh R, Cerone N, Zimbardi F, and Valerio V. *Combustion characteristics of biodiesel saturated with pyrolysis oil for power generation in gas turbines.* Renewable Energy, 2016. **99**: p. 443-451.

[17] Kurji H, Valera-Medina A, Okon A, and Chong CT. *Combustion and emission performance of CO2/CH4/biodiesel and CO2/CH4/diesel blends in a swirl burner generator.* Energy Procedia, 2017. **142**: p. 154-159.

[18] Buffi M, Valera-Medina A, Marsh R, Pugh D, Giles A, Runyon J, and Chiaramonti D. *Emissions characterization tests for hydrotreated renewable jet fuel from used cooking oil and its blends.* Applied Energy, 2017. **201**: p. 84-93.

[19] Valera-Medina A, Marsh R, Runyon J, Pugh D, Beasley P, Hughes T, and Bowen P. *Ammonia–methane combustion in tangential swirl burners for gas turbine power generation.* Applied Energy, 2017. **185**: p. 1362-1371.

[20] Chen L, Zhang Z, Lu Y, Zhang C, Zhang X, Zhang C, and Roskilly AP. *Experimental study of the gaseous and particulate matter emissions from a gas turbine combustor burning butyl butyrate and ethanol blends.* Applied Energy, 2017. **195**: p. 693-701.

[21] Bhele SK, Deshpande NV, and Thombre SB. *Experimental Investigation of Combustion Characteristics of Jatropha Biodiesel (JME) and its Diesel Blends for Gas Turbine Combustor.* Materials Today: Proceedings, 2018. **5**(11): p. 23404-23412.

[22] Buffi M, Cappelletti A, Rizzo AM, Martelli F, and Chiaramonti D. *Combustion of fast pyrolysis bio-oil and blends in a micro gas turbine.* Biomass and Bioenergy, 2018. **115**: p. 174-185.

[23] Valera-Medina A, Gutesa M, Xiao H, Pugh D, Giles A, Goktepe B, Marsh R, and Bowen P. *Premixed ammonia/hydrogen swirl combustion under rich fuel conditions for gas turbines operation.* International Journal of Hydrogen Energy, 2019. **44**(16): p. 8615-8626.

[24] Seljak T and Katrašnik T. *Emission reduction through highly oxygenated viscous biofuels: Use of glycerol in a micro gas turbine.* Energy, 2019. **169**: p. 1000-1011.

[25] Okafor EC, Somarathne KDKA, Ratthanan R, Hayakawa A, Kudo T, Kurata O, Iki N, Tsujimura T, Furutani H, and Kobayashi H. *Control of NOx and other emissions in micro gas turbine combustors fuelled with mixtures of methane and ammonia.* Combustion and Flame, 2020. **211**: p. 406-416.

[26] Agwu O, Valera-Medina A, Katrašnik T, and Seljak T. *Flame characteristics of glycerol/methanol blends in a swirl-stabilised gas turbine burner.* Fuel, 2021. **290**.

[27] Chong CT and Hochgreb S. *Flame structure, spectroscopy and emissions quantification of rapeseed biodiesel under model gas turbine conditions.* Applied Energy, 2017. **185**: p. 1383-1392.

[28] Kumar N, Varun, and Chauhan SR. *Performance and emission characteristics of biodiesel from different origins: A review.* Renewable and Sustainable Energy Reviews, 2013. **21**: p. 633-658.

[29] Wang Y, Wu J, and Lin Y. *Effects of confinement length of the central toroidal recirculation zone partly confined by the small pilot stage chamber on ignition characteristics.* Aerospace Science and Technology, 2020. **107**: p. 106277.

[30] Dimitriou P, Tsujimura T, and Suzuki Y. *Hydrogen-diesel dual-fuel engine optimization for CHP systems.* Energy, 2018. **160**: p. 740-752.
[31] Kathrotia T, Riedel U, Seipel A, Moshammer K, and Brockhinke A. *Experimental and numerical study of chemiluminescent species in low-pressure flames.* Applied Physics B, 2012. **107**(3): p. 571-584.
[32] García-Armingol T, Hardalupas Y, Taylor AMKP, and Ballester J. *Effect of local flame properties on chemiluminescence-based stoichiometry measurement.* Experimental Thermal and Fluid Science, 2014. **53**: p. 93-103.
[33] Ballester J and García-Armingol T. *Diagnostic techniques for the monitoring and control of practical flames.* Progress in Energy and Combustion Science, 2010. **36**: p. 375-411.
[34] Lefebvre AH and Ballal DR. *Gas Turbine Combustion: Alternative fuels and emissions*. 3rd ed. 2010: CRC Press Taylor & Francis Group.
[35] Alsulami R, Windell B, Nates S, Wang W, Won SH, and Windom B. *Investigating the role of atomization on flame stability of liquid fuels in an annular spray burner.* Fuel, 2020. **265**.
[36] Ballester J, Hernández R, Sanz A, Smolarz A, Barroso J, and Pina A. *Chemiluminescence monitoring in premixed flames of natural gas and its blends with hydrogen.* Proceedings of the Combustion Institute, 2009. **32**(2): p. 2983-2991.
[37] Han D-S, Kim G-B, Kim H-S, and Jeon C-H. *Experimental study of NOx correlation for fuel staged combustion using lab-scale gas turbine combustor at high pressure.* Experimental Thermal and Fluid Science, 2014. **58**: p. 62-69.